Application of H_2/H_∞ Technique to Aircraft Landing Control

Mihai Lungu[1], Romulus Lungu[2]

[1] University of Craiova, Faculty of Electrical Engineering, 107 Decebal Blvd., Craiova, Romania, Lma1312@yahoo.com
[2] University of Craiova, Faculty of Electrical Engineering, 107 Decebal Blvd., Craiova, Romania, rlungu@elth.ucv.ro

The paper presents the automatic control of the aircraft in the longitudinal plane during landing, taking into account the sensor errors and disturbances. Aircraft auto-landing is achieved by combining the H_2 and H_∞ control techniques; this way, a robust H_2/H_∞ controller is obtained. It provides good precision tracking and robust stability with respect to the uncertainties caused by different disturbances and noise type signals. The weights of the H_2 and H_∞ control techniques within the robust H_2/H_∞ controller are adjusted such that the aircraft accurately tracks the desired trajectory during the two main stages of the landing process. The design of the new automatic landing system and the robust controller also includes an optimal observer and a dynamic compensator. The theoretical results are validated by numerical simulations for the landing of a Boeing; the results are very good (Federal Aviation Administration accuracy requirements for Category III are met) and prove the robustness of the new auto-landing system even in the presence of disturbances and sensor errors.

Key words: Aircraft landing, H_2/H_∞ control, Glide slope, Flare, Sensor errors

1. Introduction

A. Antecedents and motivations

The control of aircraft during landing is a problem of both theoretical and practical interest because it is well known that landing is the most challenging among all flight phases. During landing, accidents are more likely to happen because the aircraft flies at a considerable low altitude and low speed and because of wind turbulences, wind shears, measurement noises, and so on [1]; that is why, robustness to these disturbances is the main challenge in the design of Automatic Landing Systems (ALSs). Furthermore, these ALSs must consistently control aircraft to an accurate touchdown point and a smooth touchdown to prevent its damage. In the design process, one can use different conventional control laws as: proportional-derivative (PD), proportional-integral (PI), proportional-integral-derivative (PID) for the altitude and descent velocity control [2-5], PD or PID conventional laws for the pitch angle's and pitch rate's control, as well as different laws based on the state vector, dynamic inversion concept, with command filters, dynamic compensators, and state observers [1, 6-10]. The classical PID controllers cannot track satisfyingly the desired landing trajectory and velocity, especially when there is full of disturbances and uncertainties in flight, such as the ground effect and atmospheric disturbances; therefore, the robust controllers took people's attention [11]. Thus, in recent years, lots of scientific researchers have applied the intelligent concepts for the automatic landing of aircraft; they used the optimal synthesis H_2, H_∞, H_2/H_∞ [5, 12], the adaptive synthesis based on dynamic inversion theory and neural networks theory [13-15], quantitative feedback theory [16], sliding mode control [17], linear quadratic optimal control (LQR/LQG), structured singular value μ-synthesis, or fuzzy techniques [18, 19]. Feed-forward neural networks with back propagation learning algorithm have also been used [8], the main drawback of such systems being that the neural networks require a priori training on normal and faulty operating data. In [20] the feedback linearization method has been used for nonlinear control in the design of an automatic landing system; unfortunately, the paper presents limited insight into the performance of simulations of this controller and no tests are performed outside of these simulations. In the work of Singh and Padhi [4] a nonlinear control has been designed using the dynamic inversion approach for the automatic landing of unmanned aerial vehicles along with associated path planning. The obtained algorithm is not tested in the presence of sensor errors and external disturbances,

this being a disadvantage of the algorithm. In the research area of optimal synthesis, Shue and Agarwal [11] have developed a mixed technique for the H_2/H_∞ control of landing, while Ochi and Kanai [21] have used the H_∞ control technique to design an approach for aircraft automatic landing. In these papers, the authors did not analyze the robustness of the designed controllers in the presence of sensor errors and external disturbances – issue which is considered in our paper.

B. Main contribution

This paper focuses on the automatic control of aircraft in the longitudinal plane, during landing, by using its longitudinal dynamics, taking into consideration the errors of the sensors and other different disturbances. Our aim is to design a new landing control system in the longitudinal plane by using the H_2 and H_∞ control techniques; this way, a mixed H_2/H_∞ controller is obtained. According to the authors of this paper, little progress has been reported for the landing flight control systems in the longitudinal plane by using the H_2/H_∞ approach; this motivates the present study.

The ALS designed in this paper represents an improved version of the automatic landing system designed in [6] and it differs from other similar automatic landing systems from the specialty literature; thus, our new ALS has some additional elements with respect to the one presented in [6]: 1) the mixed H_2/H_∞ optimization formulation is used instead of H_∞ optimization approach which deals with bounded exogenous signals; 2) an optimal observer is used for the estimation of the aircraft state in the presence of sensor errors and external disturbances; 3) a dynamic compensator providing one of the two components of the mixed H_2/H_∞ control law; 4) a subsystem which models the geometry of landing and provides the imposed value of the aircraft pitch angle. The inputs of the dynamic compensator are the errors in longitudinal velocity and pitch angle, while the output is the first component of the control law; the second component of the control law will be determined by using the mixed H_2/H_∞ approach and an optimization algorithm borrowed from [11]. Our new automatic landing system differs from other ALSs by a greater degree of generality, applicability, and simplicity.

2. Aircraft Dynamics and Landing Geometry

A. The geometry of landing

There are three phases in a typical landing procedure: initial approach, glide slope, and flare [22]. During initial approach, the pilot descends from the cruise altitude to an altitude of approximately 420 m above the ground for heavy aircraft or less than 420 m for light aircraft. The pilot then positions the airplane so that it is on a heading towards the runway centerline. When the aircraft approaches the outer airport marker, which is about 4 nautical miles from the runway, the glide slope path signal is intercepted [15]. As the airplane descends along the glide slope path, its pitch, attitude, and speed must be controlled; the aircraft maintains a constant speed along the flight path. The descent rate, for a Boeing 747, must be 3 m/s and the pitch angle is between -5 and 5 degrees. As the airplane descends to 7-30 m above the ground (the maximum value is for Boeing 747), the slope angle control system is disengaged and a flare maneuver is executed. The vertical descent rate is slightly decreased so that the landing gear may be able to dissipate the energy of the impact at landing. The pitch angle of the airplane is then adjusted, between 0 to 5 degrees for most aircraft, to allow a soft touchdown on the runway surface [15].

Aircraft landing is simplified if the aircraft motion in lateral plane is made without errors (deviation of the aircraft from the runway direction is zero). This is why the system for the automatic control of the flight direction is very important. Before the start of the two landing main stages in longitudinal plane (the glide slope phase and the flare phase), the pilot must cancel the aircraft lateral deviation with respect to the runway. This can be achieved by means of different control systems for the flight direction control with radio navigation subsystem and equipment used for the measurement of the distance between the aircraft and the radio markers [13, 16, 23, 24].

For the ***glide slope phase*** ($H \geq H_0$, H_0 – the altitude at which the glide slope phase ends and the second landing phase begins), the imposed (calculated) altitude H_c and the real altitude H are, respectively:

$$\dot{H}_c = V_0 \sin\gamma_c, \dot{H} \cong V_0(\theta - \alpha), \tag{1}$$

with γ_c – the imposed slope angle of aircraft's trajectory during this first stage of landing $(\gamma_c = -2.5\,\text{deg})$, V_0 – the nominal flight speed, α – the aircraft attack angle, θ – the aircraft pitch angle.

The equations associated to the ***flare phase*** $(H < H_0)$ are:

$$\dot{H}_c = -\frac{1}{\tau}(H - H_{ref}), H_c = H - H_{ref}, \tag{2}$$

where $H_{ref} = H_0 \exp(-t/\tau)$ is the reference altitude, while τ is the time constant that defines the exponential curve (flare landing phase). By integration of the above equation, one obtains:

$$H_c = H_0 - \frac{1}{\tau}\int_0^{t_c}(H - H_{ref})\mathrm{d}t = H_0 - \frac{1}{\tau}\int_0^{t_c} H_c(t)\mathrm{d}t. \tag{3}$$

This equation expresses that, for the elimination of the tracking error associated to the altitude during the flare phase, one must use an ideal integrator after the tracking error, i.e. a state which expresses the integration of aircraft altitude [25]; this will be detailed latter in this section. Now, by using the equations (1) and (2), one can calculate the imposed value (the reference value) of the aircraft pitch angle $(\bar{\theta})$ for the two stages of landing:

$$\bar{\theta} = \alpha + \frac{\dot{H}}{V_0} \cong \begin{cases} \alpha + \gamma_c, H \geq H_0, \\ \alpha + \dfrac{1}{V_0\tau}(H_{ref} - H), H < H_0. \end{cases} \tag{4}$$

B. Linearized dynamics of aircraft in longitudinal plane

The linearization of an aircraft's nonlinear dynamics is generally based on the small disturbances' method with respect to an equilibrium trajectory, usually associated with the sea level; the dynamics used in this paper belongs to a Boeing 747. The linear model of aircraft's motion, in longitudinal plane, is described by the state equation [2, 3]:

$$\dot{\boldsymbol{x}} = A\boldsymbol{x} + B\boldsymbol{u} + G\boldsymbol{u}_w, \tag{5}$$

with $\boldsymbol{x} \in R^{4\times 1}$ – the state vector, $\boldsymbol{x} = [u \quad w \quad q \quad \theta]^T, \boldsymbol{u} \in R^{2\times 1}$ – the command vector, $\boldsymbol{u} = [\delta_e \quad \delta_T]^T$, while $\boldsymbol{u}_w$ is the vector of disturbances; in equation (5), u is the longitudinal velocity, w – the vertical velocity, q – the pitch angular rate, θ - the pitch angle, while δ_e and δ_T are the elevator's deflection and the engine's command, respectively. Taking into account that the vertical velocity w is much smaller than u, aircraft's velocity in longitudinal plane can be approximated as follows: $V = \sqrt{u^2 + w^2} \cong u$; thus, the nominal value of V is considered to be $V_0 \cong u(0) = u_0$. The matrices $A \in R^{4\times 4}, B \in R^{4\times 2}$ are, respectively [7]:

$$A = \begin{bmatrix} a_{11} & a_{12} & 0 & a_{14} \\ a_{21} & a_{22} & a_{23} & a_{24} \\ a_{31} & a_{32} & a_{33} & a_{34} \\ 0 & 0 & 1 & 0 \end{bmatrix}, B = \begin{bmatrix} b_{11} & b_{12} \\ b_{21} & b_{22} \\ b_{31} & b_{32} \\ 0 & 0 \end{bmatrix}. \tag{6}$$

If we consider, as new states, the deflections δ_e and δ_T (outputs of the actuators), satisfying the equations:

$$\dot{\delta}_e = -\frac{1}{T_e}\delta_e + \frac{1}{T_e}\delta_{ec}, \dot{\delta}_T = -\frac{1}{T_T}\delta_T + \frac{1}{T_t}\delta_{Tc}, \tag{7}$$

the new state of the system becomes $\boldsymbol{x} = \begin{bmatrix} \dfrac{u}{V_0} & \dfrac{w}{V_0} & q & \theta & \delta_e & \delta_T \end{bmatrix}^T$, while the new command vector is

$\boldsymbol{u} = [\delta_{ec} \quad \delta_{Tc}]^T$; δ_{ec} and δ_{Tc} are the commands applied to elevator and to engines, respectively. Therefore, for $\boldsymbol{u_w} = 0$, the aircraft state equations are:

$$\begin{aligned}
&\frac{\dot{u}}{V_0} = a_{11}\frac{u}{V_0} + a_{12}\frac{w}{V_0} + \frac{a_{14}}{V_0}\theta + \frac{b_{11}}{V_0}\delta_e + \frac{b_{12}}{V_0}\delta_T\,,\ \frac{\dot{w}}{V_0} = a_{21}\frac{u}{V_0} + a_{22}\frac{w}{V_0} + \frac{a_{23}}{V_0}q + \frac{a_{24}}{V_0}\theta + \frac{b_{21}}{V_0}\delta_e + \frac{b_{22}}{V_0}\delta_T\,,\\
&\dot{q} = V_0 a_{31}\frac{u}{V_0} + V_0 a_{22}\frac{w}{V_0} + a_{33}q + a_{34}\theta + b_{31}\delta_e + b_{32}\delta_T\,,\ \dot{\theta} = q,\ \dot{\delta}_e = -\frac{1}{T_e}\delta_e + \frac{1}{T_e}\delta_{ec}\,,\ \dot{\delta}_T = -\frac{1}{T_T}\delta_T + \frac{1}{T_t}\delta_{Tc}\,.
\end{aligned} \tag{8}$$

For the control of aircraft during the glide slope phase, the state $\boldsymbol{x} \in R^{8\times 1}$ is chosen as follows:

$$\boldsymbol{x} = \left[\frac{u}{V_0} \quad \alpha \quad q \quad \theta \quad \frac{H}{V_0} \quad \frac{\dot{H}}{V_0} \quad \delta_e \quad \delta_T\right]^T, \tag{9}$$

with $\alpha \cong w/V_0$. Thus, one adds to equations (8) the differential equations associated to the variables H/V_0 and $\dot{H}/V_0$;

$$\frac{\dot{H}}{V_0} \cong \theta - \alpha,\ \frac{\ddot{H}}{V_0} = -a_{21}\frac{u}{V_0} - a_{22}\alpha + \left(1 - \frac{a_{23}}{V_0}\right)q - \frac{a_{24}}{V_0}\theta - \frac{b_{21}}{V_0}\delta_e - \frac{b_{22}}{V_0}\delta_T\,; \tag{10}$$

the last one has been obtained by derivation with respect to time of the first equation (10), with $\dot{\alpha} = \dot{w}/V_0$ of form (8).

Putting together equations (8) and (10), with the state vector (9), one obtains the matrices *A* and *B*;

$$A = \begin{bmatrix}
a_{11} & a_{12} & 0 & \frac{a_{14}}{V_0} & 0 & 0 & \frac{b_{11}}{V_0} & \frac{b_{12}}{V_0}\\
a_{21} & a_{22} & \frac{a_{23}}{V_0} & \frac{a_{24}}{V_0} & 0 & 0 & \frac{b_{21}}{V_0} & \frac{b_{22}}{V_0}\\
V_0 a_{31} & V_0 a_{32} & a_{33} & a_{34} & 0 & 0 & b_{31} & b_{32}\\
0 & 0 & 1 & 0 & 0 & 0 & 0 & 0\\
0 & -1 & 0 & 1 & 0 & 0 & 0 & 0\\
-a_{21} & -a_{22} & \left(1 - \frac{a_{23}}{V_0}\right) & -\frac{a_{24}}{V_0} & 0 & 0 & -\frac{b_{21}}{V_0} & -\frac{b_{22}}{V_0}\\
0 & 0 & 0 & 0 & 0 & 0 & -\frac{1}{T_e} & 0\\
0 & 0 & 0 & 0 & 0 & 0 & 0 & -\frac{1}{T_T}
\end{bmatrix}, B = \begin{bmatrix}
0 & 0\\ 0 & 0\\ 0 & 0\\ 0 & 0\\ 0 & 0\\ 0 & 0\\ \frac{1}{T_e} & 0\\ 0 & \frac{1}{T_T}
\end{bmatrix}. \tag{11}$$

Denoting with $\boldsymbol{u_w} = [u_g/V_0 \quad \alpha_g \quad q_g \quad \theta_g]^T$ – the vector of disturbances, additionally introduced in the equations of the states $u/V_0, \alpha, q, \theta,$ one yields the matrix *G* as follows:

$$G^T = \begin{bmatrix}
a_{11} & a_{21} & V_0 a_{31} & 0 & 0 & -a_{21} & 0 & 0\\
a_{12} & a_{22} & V_0 a_{32} & 0 & -1 & -a_{22} & 0 & 0\\
0 & a_{23}/V_0 & a_{33} & 1 & 0 & (1 - a_{23}/V_0) & 0 & 0\\
a_{14}/V_0 & a_{24}/V_0 & a_{34} & 0 & 1 & -a_{24}/V_0 & 0 & 0
\end{bmatrix}. \tag{12}$$

For the control of aircraft during flare, the following state $\boldsymbol{x} \in R^{8\times 1}$ is chosen:

$$\boldsymbol{x} = \left[\frac{u}{V_0} \quad \alpha \quad q \quad \theta \quad \frac{H}{V_0} \quad \frac{1}{V_0}\int H_c \quad \delta_e \quad \delta_T\right]^T; \tag{13}$$

the matrix *A* is obtained with (11), modifying only the sixth line, while the matrix *B* is the same with the one in (11); thus, one yields:

$$A=\begin{bmatrix} a_{11} & a_{12} & 0 & \frac{a_{14}}{V_0} & 0 & 0 & \frac{b_{11}}{V_0} & \frac{b_{12}}{V_0} \\ a_{21} & a_{22} & \frac{a_{23}}{V_0} & \frac{a_{24}}{V_0} & 0 & 0 & \frac{b_{21}}{V_0} & \frac{b_{22}}{V_0} \\ V_0 a_{31} & V_0 a_{32} & a_{33} & a_{34} & 0 & 0 & b_{31} & b_{32} \\ 0 & 0 & 1 & 0 & 0 & 0 & 0 & 0 \\ 0 & -1 & 0 & 1 & 0 & 0 & 0 & 0 \\ 0 & 0 & 0 & 0 & 1 & 0 & 0 & 0 \\ 0 & 0 & 0 & 0 & 0 & 0 & -\frac{1}{T_e} & 0 \\ 0 & 0 & 0 & 0 & 0 & 0 & 0 & -\frac{1}{T_T} \end{bmatrix}, B=\begin{bmatrix} 0 & 0 \\ 0 & 0 \\ 0 & 0 \\ 0 & 0 \\ 0 & 0 \\ 0 & 0 \\ \frac{1}{T_e} & 0 \\ 0 & \frac{1}{T_T} \end{bmatrix}. \quad (14)$$

3. Design of the H_2/H_∞ Control Law and of the new ALS

A. Design of the H_2/H_∞ control law

Optimal control problems have became more and more important in the design of modern engineering systems [26-29]. The solving of an optimal problem means to determine a system's input which optimizes a given cost functional and satisfies a set of constraints [27]. The control input that yields an extreme of the cost functional is known as *the optimal control* and the corresponding variation of the state variables is called *the optimal trajectory*. Some simple optimal control problems can be solved analytically, while different direct methods [30] are used to approximate the solution in the case of general optimal control problems.

In this section, the control of aircraft's flight during the two landing phases is achieved by designing a H_2/H_∞ controller. For the design process, the output controlled variables are chosen as $z_0 = \dot{H}$ and $z_1 = \ddot{H}$, respectively; the equations associated to these two variables are:

$$z_0 = C_0 \boldsymbol{x} + D_{01}\boldsymbol{u}, z_1 = C_1 \boldsymbol{x} + D_{11}\boldsymbol{u}, \quad (15)$$

while the expression of the second output variable $\left(z_1 = \ddot{H}\right)$ is:

$$\ddot{H} = V_0 q - \dot{w} = -V_0 a_{21}\frac{u}{V_0} - V_0 a_{22}\frac{w}{V_0} + V_0\left(1-\frac{a_{23}}{V_0}\right)q - a_{24}\theta - b_{21}\delta_e - b_{22}\delta_T . \quad (16)$$

For the first phase of landing (glide slope), taking into account the equation $\dot{H} \cong -V_0\alpha + V_0\theta$, we obtain:

$$\begin{aligned} &C_0 = \begin{bmatrix} 0 & -V_0 & 0 & V_0 & 0 & 0 & 0 & 0 \end{bmatrix}, D_{01} = \begin{bmatrix} c_1 & 0 \end{bmatrix}, \\ &C_1 = \begin{bmatrix} -V_0 a_{21} & -V_0 a_{22} & -V_0\left(1-\frac{a_{23}}{V_0}\right) & -a_{24} & 0 & 0 & -b_{21} & -b_{22} \end{bmatrix}, D_{11} = \begin{bmatrix} 0 & c_2 \end{bmatrix}; \end{aligned} \quad (17)$$

c_1 and c_2 are positive constants. Also, the equation of the measurement system is:

$$y = C\boldsymbol{x} + D_{22}e, \quad (18)$$

where $D_{22} = \bar{k}I_7$ ($\bar{k}$ – positive constant) is the matrix of weights associated to the vector containing the sensor errors [11]: $e = \begin{bmatrix} e_u & e_\alpha & e_q & e_\gamma & e_H & e_{\delta_e} & e_{\delta_T} \end{bmatrix}^T$, $y = \begin{bmatrix} u & \alpha & q & \gamma & H & \delta_e & \delta_T \end{bmatrix}^T$, while the matrix C is obtained by identification;

$$C=\begin{bmatrix} V_0 & 0 & 0 & 0 & 0 & 0 & 0 & 0 \\ 0 & 1 & 0 & 0 & 0 & 0 & 0 & 0 \\ 0 & 0 & 1 & 0 & 0 & 0 & 0 & 0 \\ 0 & -1 & 0 & 1 & 0 & 0 & 0 & 0 \\ 0 & 0 & 0 & 0 & V_0 & 0 & 0 & 0 \\ 0 & 0 & 0 & 0 & 0 & 0 & 1 & 0 \\ 0 & 0 & 0 & 0 & 0 & 0 & 0 & 1 \end{bmatrix}. \tag{19}$$

For the second phase of landing (flare), the equations (17) become:

$$C_0=\begin{bmatrix}0 & 0 & 0 & 0 & -V_0/\tau & 0 & 0 & 0\end{bmatrix}, C_1=\begin{bmatrix}0 & 0 & 0 & 0 & -V_0/\tau^2 & 0 & 0 & 0\end{bmatrix}, D_{01}=\begin{bmatrix}c_1 & 0\end{bmatrix}, D_{11}=\begin{bmatrix}0 & c_2\end{bmatrix}; \tag{20}$$

the matrices C_0 and C_1 have been deduced by means of equations (2). The controlled output variables z_0 and z_1 are now:

$$z_0=\dot{H}_c=-\frac{1}{\tau}H_c\cong\frac{1}{\tau}\left(H-H_{ref}\right)\cong-\frac{V_0}{\tau}\cdot\frac{H}{V_0},\ z_1=\ddot{H}=\dot{H}_c=\frac{V_0}{\tau^2}\cdot\frac{H_c}{V_0}\cong\frac{V_0}{\tau^2}\cdot\frac{H}{V_0}. \tag{21}$$

The system measurement equation is again (18), with $e=\begin{bmatrix}e_u & e_\alpha & e_q & e_\theta & e_H & e_{\delta_e} & e_{\delta_T}\end{bmatrix}^T$, $y=\begin{bmatrix}u & \alpha & q & \theta & H & \delta_e & \delta_T\end{bmatrix}^T$; thus, we get:

$$C=\begin{bmatrix} V_0 & 0 & 0 & 0 & 0 & 0 & 0 & 0 \\ 0 & 1 & 0 & 0 & 0 & 0 & 0 & 0 \\ 0 & 0 & 1 & 0 & 0 & 0 & 0 & 0 \\ 0 & 0 & 0 & 1 & 0 & 0 & 0 & 0 \\ 0 & 0 & 0 & 0 & V_0 & 0 & 0 & 0 \\ 0 & 0 & 0 & 0 & 0 & 0 & 1 & 0 \\ 0 & 0 & 0 & 0 & 0 & 0 & 0 & 1 \end{bmatrix}, \tag{22}$$

while D_{22} has the same expression as the one in the case of the first landing phase.

Putting together equations (5), (15), and (18), the following equation is obtained:

$$\begin{bmatrix}\dot{\boldsymbol{x}}\\ z_0\\ z_1\\ y\end{bmatrix}=\begin{bmatrix}A_{(8\times8)} & B_{(8\times2)} & G_{(8\times3)} & 0_{(8\times7)}\\ C_{0(1\times8)} & D_{01(1\times2)} & 0_{(1\times3)} & 0_{(1\times7)}\\ C_{1(1\times8)} & D_{11(1\times2)} & 0_{(1\times3)} & 0_{(1\times7)}\\ C_{(7\times8)} & 0_{(7\times2)} & 0_{(7\times3)} & D_{22(7\times7)}\end{bmatrix}\begin{bmatrix}\boldsymbol{x}\\ \boldsymbol{u}\\ \boldsymbol{u_w}\\ e\end{bmatrix}. \tag{23}$$

To proof that, in steady regime, the forms of $z_0=\dot{H}$ and $z_1=\ddot{H}$ are the same with the ones in equation (23), one has used the expansion of $z=\begin{bmatrix}z_0 & z_1\end{bmatrix}^T$ as function of $\boldsymbol{x}$ and $\boldsymbol{u}$; for $\boldsymbol{u}_0$=0, we have successively obtained the following equations:

$$z=\begin{bmatrix}z_0\\ z_1\end{bmatrix}=z(\boldsymbol{x},\boldsymbol{u})\cong\underbrace{z(\boldsymbol{x}_0,\boldsymbol{u}_0)}_{z_0}+\left(\frac{\partial z}{\partial\boldsymbol{x}}\right)_{(\boldsymbol{x}_0,0)}\Delta\boldsymbol{x}+\left(\frac{\partial z}{\partial\boldsymbol{u}}\right)_{(x_0,0)}\Delta\boldsymbol{u}\cong z_0+\underbrace{\begin{bmatrix}\frac{\partial z_0}{\partial x_1} & \cdots & \frac{\partial z_0}{\partial x_n}\\ \frac{\partial z_1}{\partial x_1} & \cdots & \frac{\partial z_1}{\partial x_n}\end{bmatrix}_{(\boldsymbol{x}_0,0)}}_{\begin{bmatrix}C_0\\ C_1\end{bmatrix}}\Delta\boldsymbol{x}+\underbrace{\begin{bmatrix}\frac{\partial z_0}{\partial u_1} & \frac{\partial z_0}{\partial u_2}\\ \frac{\partial z_1}{\partial u_1} & \frac{\partial z_1}{\partial u_2}\end{bmatrix}_{(\boldsymbol{x}_0,0)}}_{\begin{bmatrix}D_{01}\\ D_{11}\end{bmatrix}}\Delta\boldsymbol{u}\Leftrightarrow$$

$$\Leftrightarrow\Delta z\cong\begin{bmatrix}C_0\\ C_1\end{bmatrix}\Delta\boldsymbol{x}+\begin{bmatrix}D_{01}\\ D_{11}\end{bmatrix}\Delta\boldsymbol{u}\Leftrightarrow z\cong\begin{bmatrix}C_0\\ C_1\end{bmatrix}\boldsymbol{x}+\begin{bmatrix}D_{01}\\ D_{11}\end{bmatrix}\boldsymbol{u}\cong\overline{C}\,\boldsymbol{x}+\overline{D}\boldsymbol{u},\ \text{where}\ C_0=\begin{bmatrix}\frac{\partial z_0}{\partial x_1} & \cdots & \frac{\partial z_0}{\partial x_n}\end{bmatrix}_{(\boldsymbol{x}_0,0)},C_1=\begin{bmatrix}\frac{\partial z_1}{\partial x_1} & \cdots & \frac{\partial z_1}{\partial x_n}\end{bmatrix}_{(\boldsymbol{x}_0,0)},$$

$x_i\left(i=\overline{1,8}\right)$ are the system's states, $u_i\left(i=\overline{1,2}\right)$ are the system's inputs $\left(\delta_{ec},\delta_{Tc}\right), D_{01}=\begin{bmatrix}\frac{\partial z_0}{\partial u_1} & \frac{\partial z_0}{\partial u_2}\end{bmatrix}_{(\boldsymbol{x}_0,0)}=$

$$= \left[\frac{\partial \dot{H}}{\partial \delta_{e_c}} \quad \frac{\partial \dot{H}}{\partial \delta_{T_c}} \right]_{(\boldsymbol{x}_0, 0)} = [c_1 \quad 0], D_{11} = \left[\frac{\partial z_1}{\partial u_1} \quad \frac{\partial z_1}{\partial u_2} \right]_{(\boldsymbol{x}_0, 0)} = \left[\frac{\partial \ddot{H}}{\partial \delta_{e_c}} \quad \frac{\partial \ddot{H}}{\partial \delta_{T_c}} \right]_{(\boldsymbol{x}_0, 0)} = [0 \quad c_2], \overline{C} = \begin{bmatrix} C_0 \\ C_1 \end{bmatrix}, \overline{D} = \begin{bmatrix} D_{01} \\ D_{11} \end{bmatrix}.$$

The control law $\boldsymbol{u}$ is calculated by using the formula:

$$\boldsymbol{u} = \hat{\boldsymbol{u}} + \boldsymbol{u}_{dc}, \tag{24}$$

where $\hat{\boldsymbol{u}}$ is the optimal command calculated by means of the H_2/H_∞ method, while the component $\boldsymbol{u}_{dc}$ is the output of a dynamic compensator. For the calculation of the optimal control law $\hat{\boldsymbol{u}}$ (the output of the H_2/H_∞ controller) we have to minimize two cost functionals. The first one, associated to the H_2 approach, is:

$$J_0 = \frac{1}{2} \int_0^\infty z_0^T z_0 \mathrm{d}t = \frac{1}{2} \int_0^\infty \left[\boldsymbol{x}^T \underbrace{\left(C_0^T C_0 \right)}_{Q_0} \boldsymbol{x} + \hat{\boldsymbol{u}}^T \underbrace{\left(D_{01}^T D_{01} \right)}_{R_0} \hat{\boldsymbol{u}} \right] \mathrm{d}t. \tag{25}$$

In the case of H_2 approach, the optimal control law has the form [31]:

$$\hat{\boldsymbol{u}} = -K\hat{\boldsymbol{x}}, K = R_0^+ B^T P, R_0 = D_{01}^T D_{01}; \tag{26}$$

in the above equation, R_0^+ denotes the pseudo-inverse of the matrix R_0, the symmetric and positive defined matrix $P \in R^{8\times 8}$ is the stabilizing solution of the Riccati matriceal equation [11]:

$$A^T P + PA - PBR_0^+ B^T P + Q_0 = 0, \tag{27}$$

with $Q_0 = C_0^T C_0$, while $\hat{\boldsymbol{x}}$ is aircraft's estimated state (provided by an observer which is designed by using the H_2 approach); to obtain this signal, one borrowed the observer presented in [31], i.e.:

$$\dot{\hat{\boldsymbol{x}}} = A\hat{\boldsymbol{x}} + B\boldsymbol{u} + L\left(y - C\hat{\boldsymbol{x}} \right); \tag{28}$$

the observer gain matrix L is calculated with the formula:

$$L = P^* C^T \left(D_{22}^T D_{22} \right)^{-1}, \tag{29}$$

where P^* is the stabilizing solution of the Riccati matriceal equation [11]:

$$AP^* + P^* A^T - P^* C^T \left(D_{22}^T D_{22} \right)^{-1} CP^* + GG^T = 0. \tag{30}$$

The H_∞ control method combines the classical shaping with robust stabilization; using now this control approach, the system state equation, the equation of the output variable z_1, and the measurement equation of the system, for the two stages of landing, we calculate the optimal control law $\hat{\boldsymbol{u}}$ which minimizes the cost functional:

$$J_1 = \frac{1}{2} \int_0^\infty z_1^T z_1 \mathrm{d}t = \frac{1}{2} \int_0^\infty \left[\boldsymbol{x}^T \underbrace{\left(C_1^T C_1 \right)}_{Q_1} \boldsymbol{x} + \hat{\boldsymbol{u}}^T \underbrace{\left(D_{11}^T D_{11} \right)}_{R_1} \hat{\boldsymbol{u}} \right] \mathrm{d}t. \tag{31}$$

In this case, the optimal control law has the form [31]:

$$\hat{\boldsymbol{u}} = -K_\infty \hat{\boldsymbol{x}}, K_\infty = R_1^+ B^T P_\infty, R_1 = D_{11}^T D_{11}; \tag{32}$$

R_1^+ denotes the pseudo-inverse of the matrix R_1, while the symmetric and positive defined matrix $P_\infty \in R^{8\times 8}$ is the stabilizing solution of the Riccati matriceal equation [11]:

$$A^T P_\infty + P_\infty A - P_\infty \left(BR_1^+ B^T - \mu_1^{-2} GG^T \right) P_\infty + Q_1 = 0, \tag{33}$$

where $Q_1 = C_1^T C_1$ and R_1 are positive matrices, while μ_1 is a positive scalar for which the Riccati equation (33) has a stabilizing solution. The observer equation is (28) with the gain matrix $L_\infty \in R^{8\times 7}$ having the form:

$$L_\infty = P_\infty^* C^T \left(D_{22}^T D_{22}\right)^{-1}, \tag{34}$$

where $P_\infty^* \in R^{8\times 8}$ is the solution of the Riccati matriceal equation:

$$AP_\infty^* + P_\infty^* A^T - P_\infty^* \left(C^T C - \mu_2^{-2} C_1^T C_1\right) P_\infty^* + GG^T = 0; \tag{35}$$

μ_2 is a positive scalar for which the equation (35) has a stabilizing solution.

In order to obtain an optimum for the control law calculated both with H_2 and H_∞ approaches, i.e. to obtain the expression of the H_2/H_∞ control law, the following algorithm [11] can be used:

Step 1: The determination of the norms H_2 and H_∞ associated to the solutions of the Riccati equations (27), (30), (33), and (35);

Step 2: The calculation of the matrices

$$\hat{P} = (1-k)P + kP_\infty,\ \hat{P}^* = (1-k)P^* + kP_\infty^*, \tag{36}$$

with $k \in (0,1)$; in the fourth section of the paper, we will choose k=0.5 but we will also analyze the effect of this constant's modification on the altitude deviation with respect to its nominal value;

Step 3: The check of the following conditions' fulfillment [11]:

$$\hat{P}, \hat{P}^* \geq 0, \hat{P}\hat{P}^* < I. \tag{37}$$

Step 4: The choosing of the constant k and the running of the steps 2 and 3 until the conditions (37) are met;

Step 5: The obtaining of the control law's final expression (combining the H_2 and the H_∞ approaches) by means of the equations:

$$\hat{\boldsymbol{u}} = -\hat{K}\hat{\boldsymbol{x}}, \hat{K} = R_1^+ B^T \hat{P}, \tag{38}$$

and the obtaining of the final expression for the observer gain matrix: $\hat{L} = \hat{P}^* C^T \left(D_{22}^T D_{22}\right)^{-1}$.

B. The structure of the new automatic landing system

The structure of the new automatic landing system using a H_2/H_∞ controller, a dynamic compensator, an optimal observer, and the geometry of landing is presented in Fig. 1. Here, the variables with a line above them mean the desired (imposed) values of these variables, while the matrix C_r has the form:

$$C_r = \begin{bmatrix} V_0 & 0 & 0 & 0 & 0 & 0 & 0 & 0 \\ 0 & 0 & 0 & 1 & 0 & 0 & 0 & 0 \\ 0 & 0 & 0 & 0 & V_0 & 0 & 0 & 0 \end{bmatrix}. \tag{39}$$

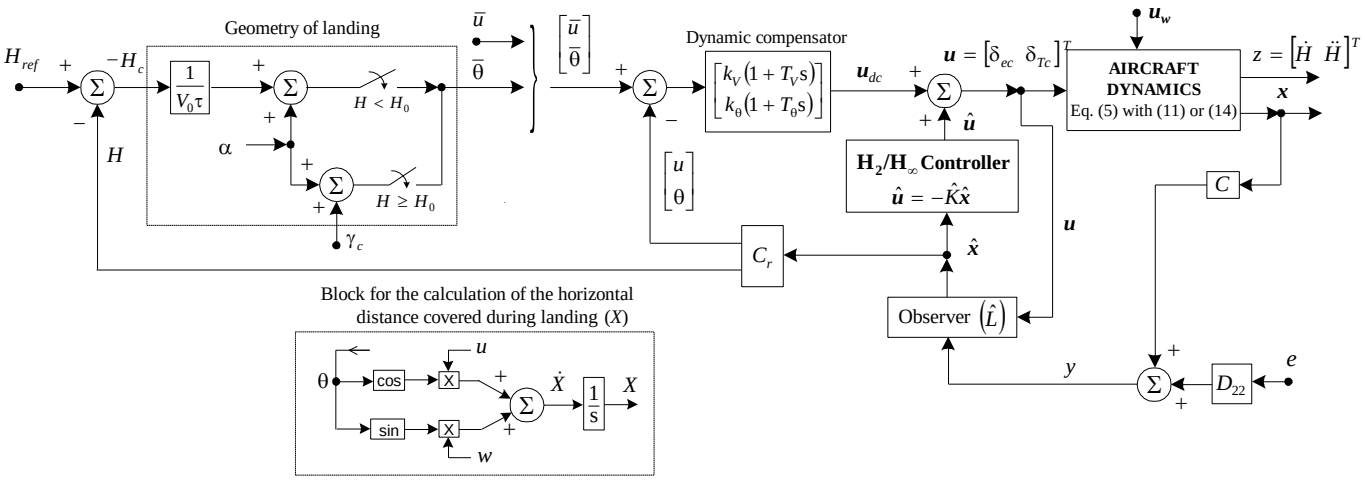

Fig. 1 H_2/H_∞ optimal control system for aircraft landing

The linear dynamic compensator is chosen as proportional-derivative one; it provides the signal $\boldsymbol{u}_{dc}$ which is necessary for the system's stabilization. The proportional coefficients (k_V and k_θ) and the derivative ones ($k_V T_V$ and $k_\theta T_\theta$) associated to the dynamic compensator may be calculated either by imposing desired roots (solutions) for the characteristic equations of the linear closed loop subsystem with negative unitary feedback or by means of the Ziegler-Nichols tuning rules.

The obtaining of the aircraft desired landing trajectory mainly involves two variables' control: the forward speed (u) and the pitch angle (θ). According to the landing requirements for Boeing 747, the aircraft must descend from the cruising altitude to a lower one (around 420 m). Meanwhile, the aircraft speed is also reduced from the cruising value to an approach value and, after that, it remains constant. So, when we choose the desired trajectory, we firstly choose the desired forward speed u. The optimal control system associated to aircraft flight during landing (longitudinal plane), based on H_2/H_∞ method, together with the optimal observer must assure the convergences: $\Delta y = y - \bar{y} \to 0 \left(y = C\boldsymbol{x} \to \bar{y} = C\bar{\boldsymbol{x}}, \boldsymbol{x} \to \bar{\boldsymbol{x}} \right), \Delta \boldsymbol{x} = \boldsymbol{x} - \bar{\boldsymbol{x}} \to 0 \left(\hat{\boldsymbol{x}} \to \boldsymbol{x} \to \bar{\boldsymbol{x}} \right)$; here, $\bar{\boldsymbol{x}}$ is the aircraft desired state, while $\bar{y}$ is the reference vector associated to the measured output y.

4. Numerical Simulation Results

A. Numerical simulation setup

To study the performances of the new obtained automatic landing system, we consider the landing of a Boeing 747. Complex simulations in Matlab/Simulink environment have been performed; thus, we designed the optimal observer, the H_2/H_∞ controller, and, after that, we validated the proposed automatic landing system. The values of the coefficients for Boeing 747 dynamics have been borrowed from [6]: $a_{11} = -0.021, a_{12} = 0.122, a_{14} = -0.322, a_{24} = 0, a_{31} = 0.017, a_{32} = -0.164, a_{33} = -0.412, a_{34} = 0, b_{11} = 0.01, b_{12} = 1,$ $b_{21} = -0.064, b_{22} = -0.044, b_{31} = -0.378, b_{32} = 0.544, V_0 = 70\,\text{m/s}, T_e = T_T = 0.9\,\text{s}, \bar{u} = V_0, \tau = 4, c_1 = 0.31, c_2 = 3.16,$ $k_V = k_\theta = 1, T_V = T_\theta = 1\,\text{s}, \mu_1 = 50, \mu_2 = 100.$ By using the equation (12), the elements of matrix G have been calculated; for the two stages of landing, the vector containing the sensor errors is $e = \left[0.1\,\text{m/s} \quad 0.1\,\text{deg} \quad 0\,\text{deg/s} \quad 0.1\,\text{deg} \quad 0\,\text{m} \quad 0.1\,\text{deg} \quad 0.1\,\text{deg} \right]^T$. For the first landing phase, the initial value of the state is $\boldsymbol{x}(0) = \left[1.0143 \quad -0.5\,\text{deg} \quad 2\,\text{deg/s} \quad -2.5\,\text{deg} \quad 6\,\text{s} \quad 0 \quad -1\,\text{deg} \quad 2\,\text{deg} \right]^T$, while, for the second phase of landing, the initial state is $\boldsymbol{x}(0) = \left[1 \quad 0\,\text{deg} \quad 0\,\text{deg/s} \quad 0\,\text{deg} \quad 0.428\,\text{s} \quad 0 \quad -2\,\text{deg} \quad -1\,\text{deg} \right]^T$. The vector of disturbances, additionally introduced in the state equations, is $\boldsymbol{u}_w = \left[-1.057 \quad 0.05 \quad 0\,\text{deg/s} \quad 2.55\,\text{deg} \right]^T$ – first landing phase, and $\boldsymbol{u}_w = \left[-1.13 \quad 0.05 \quad 0\,\text{deg/s} \quad 0\,\text{deg} \right]^T$ – second landing phase, respectively.

B. Results and discussion

In Figs. 2 and 3 we represent the time characteristics for the glide slope landing phase and flare landing phase, respectively; the characteristics have been represented for the new ALS affected by disturbances in the presence or in the absence of sensor errors (the sensors are used for the measurement of the states). The last three mini-graphics in Figs. 2 and 3 represent the deviations of the forward speed (u), slope angle (γ), and altitude (H) with respect to their nominal values, i.e. $\bar{u} - u, \gamma_c - \gamma, H_{ref} - H$. The presence of the sensor errors is not visible: the curves with solid line (obtained for the ALS without sensor errors) overlap almost perfectly over the curves plotted with dashed line (obtained for the ALS with sensor errors). The time origin for the flare trajectory is chosen zero when the altitude is H=H_0=30 m (the altitude at which the glide slope ends).

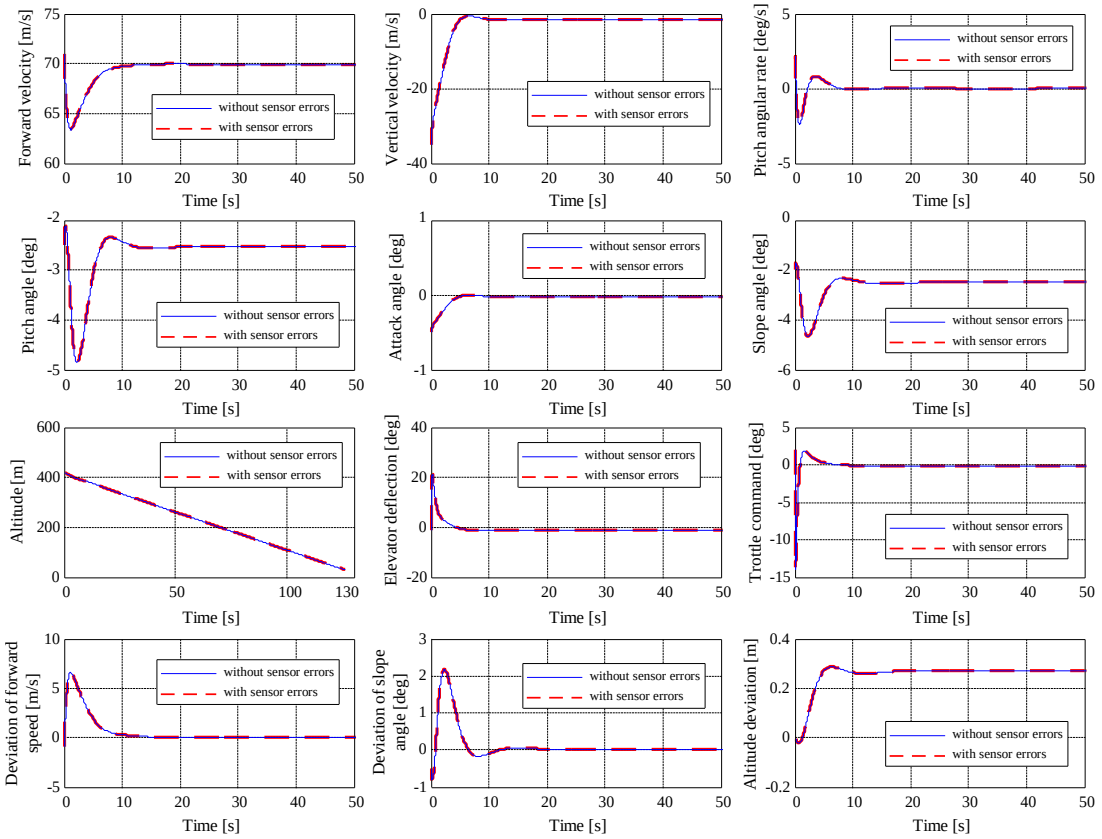

Fig. 2 Time characteristics for the glide slope phase, with or without sensor errors

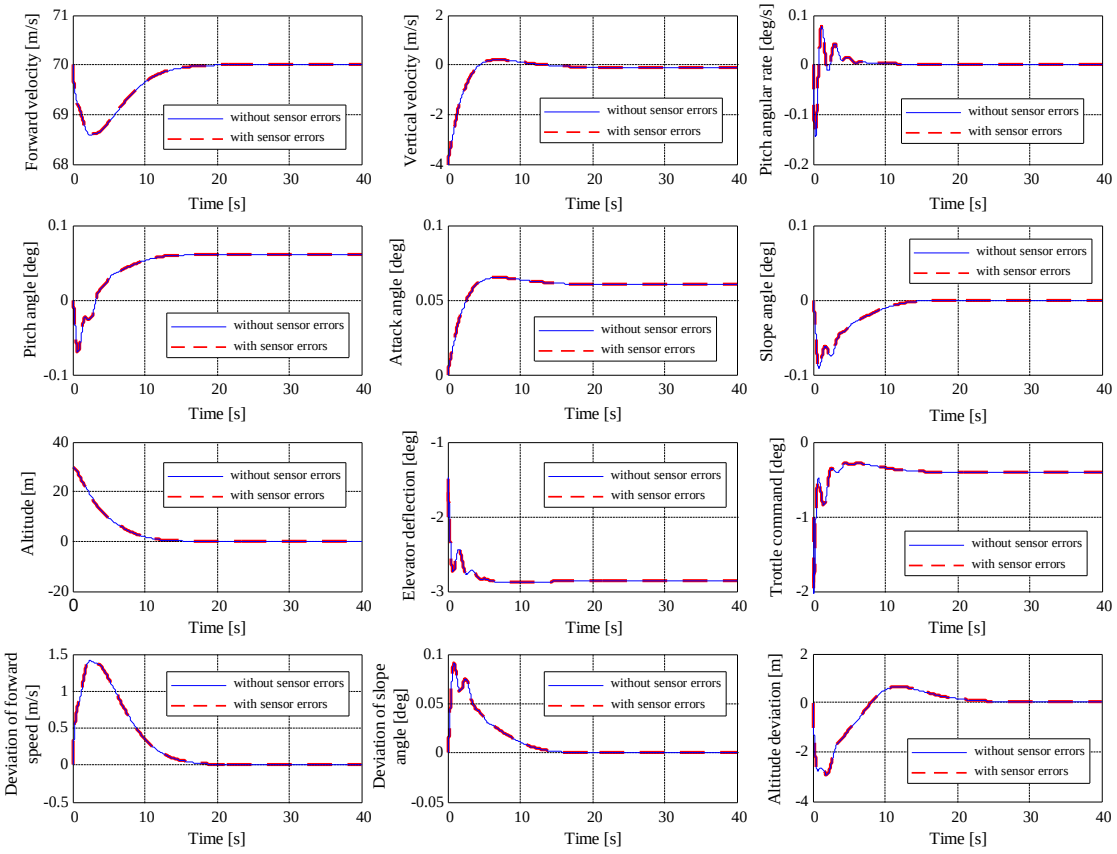

Fig. 3 Time characteristics for the flare phase, with or without sensor errors

Remark 1

From the theoretical part of this paper, we retained the mandatory values of the slope angle (the difference between the pitch angle and the attack angle): -2.5 degrees in the first landing phase and 0 degrees in the second phase, respectively. By analyzing Figs. 2 and 3, we remark the correctness of the simulation data. During the glide slope, the aircraft must have a linear descendent trajectory (7th graphic in Fig. 2) and, as a consequence, the pitch angle must be negative; as one can see in Fig. 2, the pitch angle is -2.52 degrees, while the attack angle is slightly negative $(\cong -0.02\,\text{deg})$; it results the desired slope angle (-2.5 degrees). In the flare phase, the aircraft must describe a parabolic trajectory (7th graphic in Fig. 3) with a null slope angle; as one can see in Fig. 3, the pitch and attack angles become zero in about 20 seconds; it results the desired null slope angle. □

Remark 2

The landing begins at a longitudinal speed initially exceeding the nominal speed by 1 m/s (see the first graphic in Fig. 2). The speed should be reduced to the normal speed (70 m/s) and then kept at this value; this landing process begins at 420 m (see the 7th graphic in Fig. 2). To test the robustness of the new ALS, in all simulations, we have taken into consideration the disturbances. From the last graphic in Figs. 2 and 3, we can see that the final error between the desired path and the actual path is less than 0.3 m during the glide slope phase and 0 m for the flare. These errors are very good if the Federal Aviation Administration (FAA) accuracy requirements for Category III (the best category) [32] are analyzed; according to FAA Category III accuracy requirements, the vertical error (altitude deviation with respect to its nominal value) must be less than 0.5 m, the lateral deviation must be less than 4.1 m, while the final altitude at the end of flare must be 0 m. The robustness of our new automatic landing system is guaranteed by the H_2/H_∞ control technique, this method being capable to handle the plant with measurement noise (sensor errors) and disturbances. From the forward speed's point of view, the error is less than 0.01m/s (10th graphic in Figs. 2 and 3); because the deviation of the slope angle with respect to its nominal value $(\gamma_c - \gamma)$ tends to zero (11th graphic in Figs. 2 and 3) we conclude that $\gamma \to \gamma_c = -2.5\,\text{deg}$, for the first landing phase, and $\gamma \to \gamma_c = 0\,\text{deg}$ for the second landing phase. □

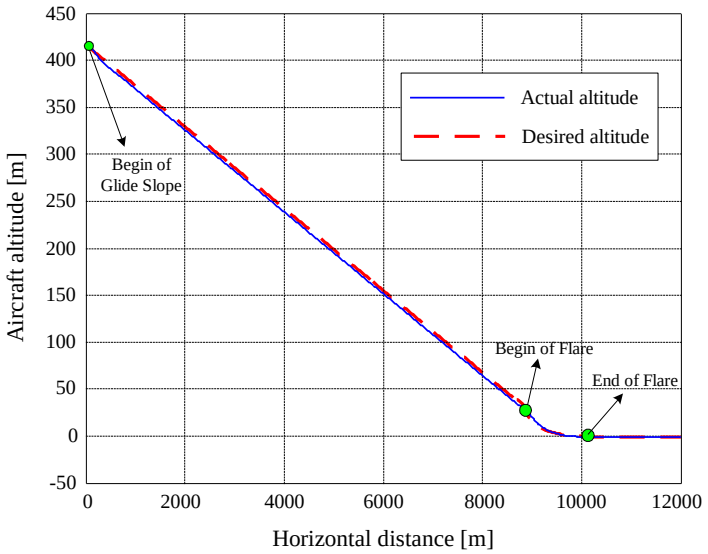

Fig. 4 Aircraft altitude versus horizontal distance

In Fig. 4, the characteristics $H(X)$ and $H_{ref}(X)$ are presented; X represents the horizontal distance covered by aircraft during landing. The optimal control system associated to aircraft flight during landing (longitudinal plane), based on H_2/H_∞ technique, assures the convergence $H \to H_{ref}$, for both cases when the sensor errors are taken or not into consideration. A little difference appears during the first landing phase (between 420 m and 30 m), but this error is canceled and it is very close to zero during flare; this error

meets the FAA Category III accuracy requirements (see the 12th graphics in Figs. 2 and 3). During the second phase of landing, the trajectory corresponds to a desired exponential curve; the point where the airplane landing gear touches the ground is approximately the same with the desired point (situated to approximately 10010 m horizontal distance from the point associated to the start of the landing). □

Remark 3

For Boeing 747, the first phase of the landing process takes approximately 126 seconds (see the 7th graphic in Fig. 2), while the second phase of landing (flare phase) takes approximately 17 seconds (see the 7th graphic in Fig. 3); in the same time, the steady values of aircraft longitudinal velocity and vertical velocity are $u \cong 70\,\text{m/s}, w \cong -1.7\,\text{m/s}$ (glide slope – Fig. 2) and $u \cong 70\,\text{m/s}, w \cong -0.3\,\text{m/s}$ (flare – Fig. 3), respectively. During the two stages of landing, the vertical velocity's mean values are $w_{mean} \cong -3.09\,\text{m/s}$ and $w_{mean} \cong -1.77\,\text{m/s}$, respectively. Using this information, we make now a brief analysis regarding the correctness of the numerical simulation data: 1) the horizontal distance covered by the aircraft in the first landing phase must be approximately $X = 70\,\text{m/s} \cdot 126\,\text{s} = 8820\,\text{m}$ – value confirmed by Fig. 4; 2) the horizontal distance covered by aircraft in the second landing phase must be approximately $X = 70\,\text{m/s} \cdot 17\,\text{s} = 1190\,\text{m}$ – value confirmed by Fig. 4; 3) the total horizontal distance covered during the whole landing process is $X = 8820 + 1190 = 10010\,\text{m}$ – value confirmed again by Fig. 4; 4) the vertical distance covered by the aircraft in the first landing phase must be approximately $3.09\,\text{m/s} \cdot 126\,\text{s} = 389.34\,\text{m}$, while the vertical distance covered in the second landing phase must be approximately $1.77\,\text{m/s} \cdot 17\,\text{s} = 30.09\,\text{m}$. These values are again confirmed by Figs. 2 and 3 since the glide slope means a 390 m descent for the aircraft's center of gravity, while the flare means a 30 m descend. □

In the third paragraph of the paper, the matrix D_{22} (the matrix of weights associated to the sensor errors) has been chosen as $D_{22} = \bar{k} I_7$ ($\bar{k}$ – positive constant, $\bar{k} = \det(D_{22})$); for Figs. 2-4, we have used the value $\bar{k} = 1$, but it is interesting to optimize this constant. According to eqs. (29) and (34), a change of the matrix D_{22} is equivalent with the modification of the observer's matrices L, L_∞, and, according to the eqs. (30), (36), and $\hat{L} = \hat{P}^* C^T \left(D_{22}^T D_{22}\right)^{-1}$, this change also means a modification of the observer's final gain matrix $\left(\hat{L}\right)$, of the observer's errors, of the matrices $P^*, \hat{P}^*$, and of all the variables' time history. □

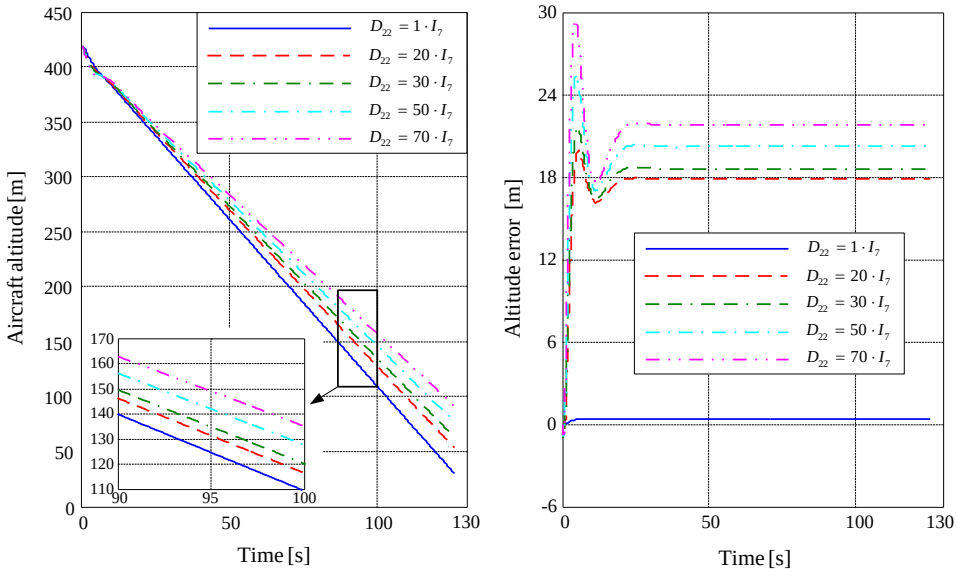

Fig. 5 Aircraft altitude and altitude errors during glide slope for different matrix D_{22}

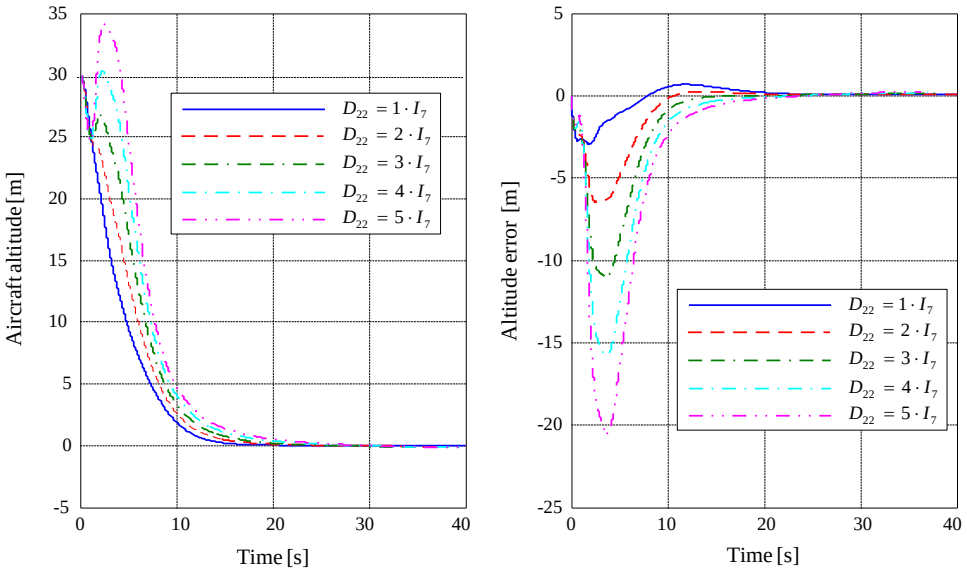

Fig. 6 Aircraft altitude and altitude errors during flare for different matrix D_{22}

Because the most important error is the altitude error, beside the aircraft altitude, we represent in Fig. 5 the time history of the altitude error $(H_{ref} - H)$ for different values of the matrix D_{22}; we have chosen 5 values for the constant $\bar{k}$, i.e.: 1, 20, 30, 50, and 70. For the first landing phase, as one can see in the first graphic in Fig. 5, the altitude decays faster for small values of the constant $\bar{k}$; this means that an increase of the D_{22} determinant is equivalent with the increase of the glide slope duration and horizontal distance covered during this first stage of landing. In the same time, the increase of the D_{22} determinant means higher altitude error (second graphic in Fig. 5). For the flare stage, in Fig. 6 we represented the time histories of the altitude and altitude error for other five values of $\bar{k}$, i.e.: 1, 2, 3, 4, and 5; these five values are smaller than the ones chosen for the glide slope because, in this stage, the altitude is more sensitive with respect to the constant $\bar{k}$. In this case, the influence of D_{22}'s modification is different; for $\bar{k} = 1$ the altitude describes an exponential curve, while the altitude decreases to zero after an important hump for the other four values (first graphic in Fig. 6). This hump (increase of the altitude followed by its decrease) cannot be accepted during flare because the aircraft may be susceptible to accidents. The modification of $\bar{k}$ does not modify the final value of the altitude error (see the second graphic in Fig. 6) but it dramatically increases its overshoot. On the other hand, the flare's duration and the horizontal distance covered during this stage of landing are not influenced by the modification of the matrix D_{22} through the constant $\bar{k}$.

In equation (36) the constant k has been chosen 0.5 but it is also interesting to analyze the effect of this constant's modification on the altitude and altitude deviation with respect to its nominal value. Actually, the constant k represents the weight of the matrices P_∞ and P_∞^*, while the constant (1-k) represents the weight of the matrices P and P^* in the matrices $\hat{P}$ and $\hat{P}^*$ calculated by means of the H_2/H_∞ technique. With other words, the constant k may be regarded as the weight of the H_∞ technique in the control law design, while the constant (1-k) may be regarded as the weight of the H_2 technique in the control law design. If k=1, the control law is designed only by using the H_∞ technique, while, if k=0, the control law is designed only by using the H_2 technique. Till now, the weights of H_2 and H_∞ techniques have been considered equal (k=1-k=0.5); now, we increase and decrease the value of constant k and we analyze which is the effect of this modification on the aircraft altitude and altitude deviation error $(H_{ref} - H)$. These characteristics, in the presence of sensor errors, are represented in Fig. 7 (glide slope) and Fig. 8 (flare).

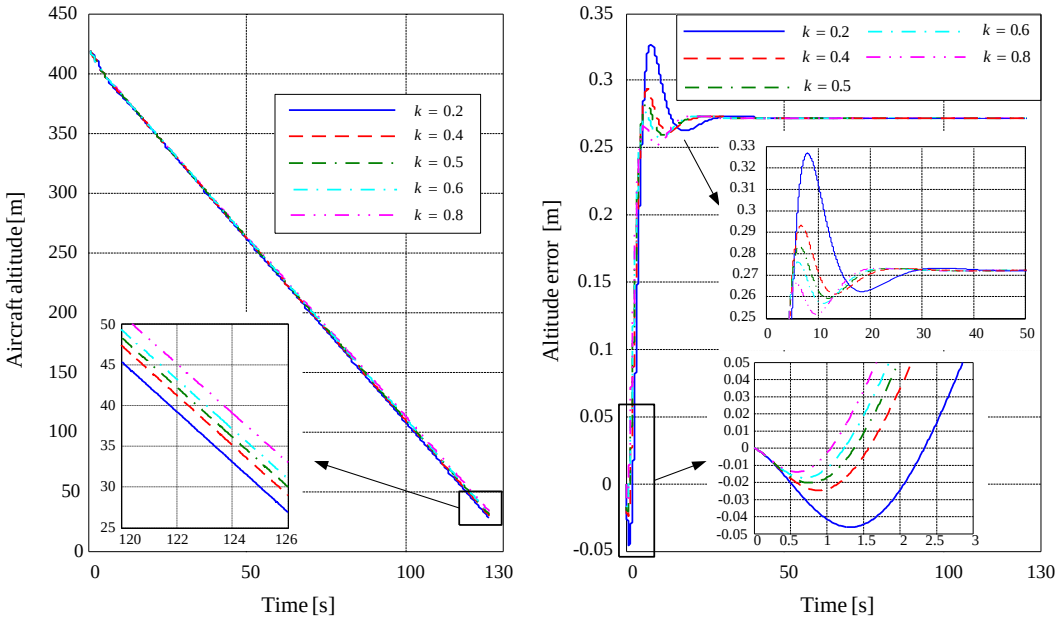

Fig. 7 Aircraft altitude and altitude errors during glide slope for different values of constant *k*

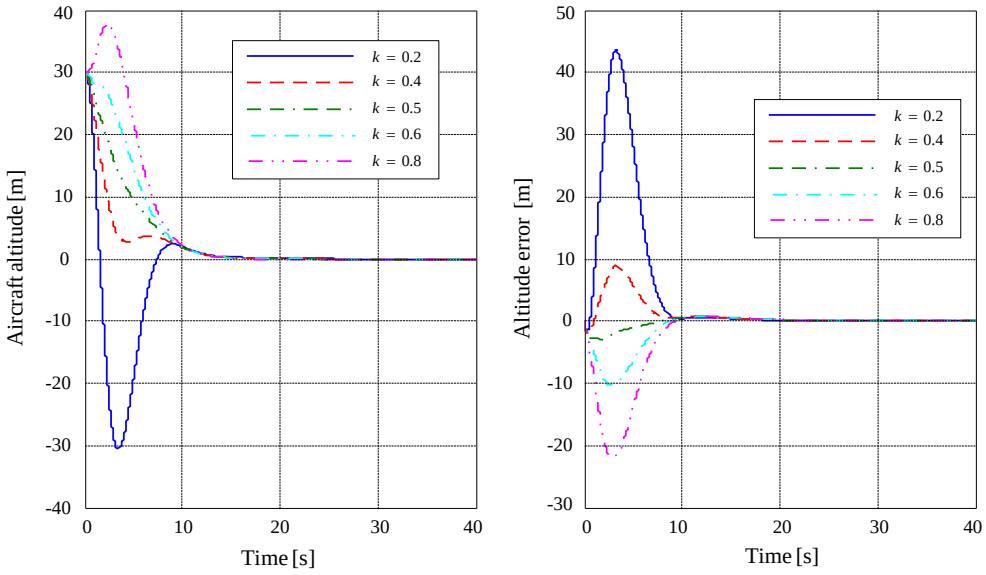

Fig. 8 Aircraft altitude and altitude errors during flare for different values of constant k

Analyzing the characteristics' family in Fig. 7, we remark that the increase of the constant *k* from 0.2 to 0.8 leads to the increase of the glide slope's duration and horizontal distance covered during this first stage of landing, the advantage being related to the fact that the overshoots and the transient regimes are smaller. Analyzing now the characteristics' family in Fig. 8 (flare phase) we remark that the exponential curve for the altitude is obtained only for k=0.5 (the weights of H_2 and H_∞ techniques are equal in the control design); increasing or decreasing the constant *k*, we notice that the altitude tends to zero after an important hump (first graphic in Fig. 8). During flare, the altitude must be described by null overshoot, this being achieved only for k=0.5. Moreover, the modification of *k* does not modify the final value of the altitude error but it dramatically increases the overshoot (see the second graphic in Fig. 8). On the other hand, the flare duration and the horizontal distance covered during this stage of landing are not influenced by the modification of the weight *k*. Concluding, the optimization process of the constant *k* leads to k=0.5.

Remark 4

The problem of landing has also been discussed in other papers, different types of ALSs being designed [1-4]. If we make a brief comparison between our ALS and the ones based on an Instrumental

Landing System or conventional/fuzzy control of flight altitude by using the system's state [3], we remark that from the system transient regime period and overshoot's points of view, the ALS based on the H_2/H_∞ technique and dynamic compensator work slightly better. Improvement of the performance was obtained by replacing the conventional controllers with fuzzy controllers [3], but those ALSs can not be used for no-bounded exogenous signals or strongly nonlinear aircraft dynamics. Our new ALS uses the mixed H_2/H_∞ technique, this having the advantage over classical control techniques in that it has applicability to problems involving multivariate systems with cross-coupling between channels; the only disadvantage is related to the non-linear constraints which are generally not well-handled. Since some of the exogenous inputs, as the sensor noises, are usually modeled by random variables, a mixed H_2/H_∞ optimization formulation is more appropriate, taking into account that the pure H_2 and H_∞ optimization approaches deal with energy bounded exogenous signals. □

5. Conclusions

Auto-landing systems provide outstanding flight control performance, a smoother landing, and increase the passengers' comfort; but there are limits: these systems work only within a specified operational safety envelope. The purpose of this study was to design a robust automatic landing system by using the H_2 and H_∞ control techniques taking into consideration the sensor errors and other different disturbances; this way, a mixed H_2/H_∞ controller has been obtained. It provides good precision tracking and robust stability with respect to the uncertainties caused by different disturbances and noise type signals. The ALS designed in this paper represents an improved version of the automatic landing system designed in [6] having some additional elements: an optimal observer providing the aircraft estimated state, a dynamic compensator providing one of the two components of the mixed H_2/H_∞ control law, and a subsystem which models the geometry of landing and provides the imposed value of the aircraft pitch angle. The design of the optimal control law gives the ALS a greater degree of generality, applicability, and simplicity. The simulation results are promising and show the robustness of the algorithm even in the presence of disturbances and sensor errors; moreover, the very small errors meet the FAA accuracy requirements for Category III.

References

[1] Liao F, Wang JL, Poh EK, Dong L. Fault-Tolerant Robust Automatic Landing Control Design, *Journal of Guidance, Control, and Dynamics*, 2005; **28** (5).

[2] Lungu R, Lungu M, Grigorie TL. ALSs with conventional and fuzzy controllers considering wind shears and gyro errors. *Journal of Aerospace Engineering*, 2012; **26** (4): 794-813.

[3] Lungu R, Lungu M, Grigorie TL. Automatic control of aircraft in longitudinal plane during landing. *IEEE Transactions on Aerospace & Electronic Systems*, 2013; **49** (2): 1338-1350.

[4] Singh S, Padhi R, Automatic Path Planning and Control Design for Autonomous Landing of UAVs using Dynamic Inversion, *American Control Conference Riverfront*, St. Louis, MO, USA , 2009; 2409-2414.

[5] Juang JG, Cheng KC. Application of Neural Network to Disturbances Encountered Landing Control, *IEEE Transactions on Intelligent Transportation Systems*, 2006; **7** (4): 582-588.

[6] Che J, Chen D. Automatic Landing Control using H-inf control and Stable Inversion, *Proceedings of the 40th Conference on Decision and Control*, Orlando, Florida, USA, 2001; 241-246.

[7] Lungu M. *Sisteme de conducere a zborului (Flight control systems*), Sitech Publisher, 2008.

[8] Pashilkar A, Sundararajan N, Saratchhandran PA. Fault-Tolerant Neural Aided controller for Aircraft Auto-Landing, *Aerospace Science and Technology*, 2006; **10** (1): 49-61.

[9] Shau-Shiun J, Gebre-Egziabher D, Walter T, Enge P. Improving GPS-based landing system performance using an empirical barometric altimeter confidence bound, *IEEE Transactions on Aerospace and Electronic Systems*, 2008; **44** (1): 127-146.

[10] Yicheng L, Zhang T, Jingyan S, Khan MJ. Controller design for high-order descriptor linear systems based on requirements on tracking performance and disturbance rejection, *Aerospace Science and Technology*, 2009; **13** (7): 364-373.

[11] Shue S, Agarwal RK. Design of automatic landing systems using mixed H_2/H_∞ control, *Journal of Guidance, Control, and Dynamics*, 1999; **2**: 103-114.

[12] Li Y, Sundararajan N, Saratchandran P, Wang Z. Robust Neuro-H∞ controller design for aircraft auto-landing, *IEEE Transactions on Aerospace and Electronic Systems*, 2004; **40** (1): 158-167.
[13] Mori R, Suzuki S. Neural Network Modeling of Lateral Pilot Landing Control, *Journal of Aircraft*, 2009; **46**: 1721-1726.
[14] Vo H, Sridhar S. Robust Control of F-16 Lateral Dynamics, *International Journal of Aerospace and Mechanical Engineering* 2008; 80-85.
[15] Juang J, Chang H, Chang W. Intelligent automatic landing system using time delay neural network controller, *Applied Artificial Intelligence: An International Journal*, 2003; **17** (7): 563-581.
[16] Wagner T, Valasek J. Digital Autoland Control Laws Using Quantitative Feedback Theory and Direct Digital Design, *Journal of Guidance, Control, and Dynamics*, 2007; **30** (5): 1399-1413.
[17] Venkateswara DM, Tiauw HG. Automatic landing system design using sliding mode control, *Aerospace Science and Technology*, 2014; **32** (1): 180-187.
[18] Zdenko K, Stjepan B. *Fuzzy Controller Design – Theory and applications*, Taylor and Francis Group, 2006.
[19] Kumar V, Rana KP, Gupt, V. Real-Time Performance Evaluation of a Fuzzy PI + Fuzzy PD Controller for Liquid-Level Process, *International Journal of Intelligent Control and Systems*, 2008; **13** (2): 89-96.
[20] Prasad B, Pradeep S. Automatic Landing System Design using Feedback Linearization Method, AIAA 2007-2733, *AIAA Infotech@Aerospace Conference and Exhibit*, Rohnert Park, California, 7-10 May 2007.
[21] Ochi Y, Kanai K. Automatic approach and landing for propulsion controlled aircraft by H∞ control *Proceedings of the 1999 IEEE International Conference on Control Applications*, Hawaii, 1999; 997-1002.
[22] Parkinson BW, O'Connor ML, Fitzgibbon KT. Aircraft automatic approach and landing using GPS, *Global Positioning System: Theory and Applications*, 1996; **II**: 397-425.
[23] Jourdan C, Marc C. Ground-Effect Identification and Autoland System Validation from Flight Data, *Journal of Aircraft*, 2004; **41** (4): 730-734.
[24] Malaek M, Izadi H, Pakmehr M. Flight Envelope Expansion in Landing Phase Using Classic, Intelligent and Adaptive Controllers, *Journal of Aircraft*, 2006; **43** (1): 91-101.
[25] Wang R, Zhou Z, Shen Y. Robust Landing Control and Simulation for Flying Wing UAV. *Proceedings of the 26th Chinese Control Conference*, China, 600-604.
[26] Lau K, Lopez R, Onate E. Neural Networks for Optimal Control of Aircraft Landing Systems, *Proceedings of the World Congress on Engineering*, 2007; **II**: 904-911.
[27] Kirk DE. *Optimal Control Theory. An Introduction*, Prentice Hall, 1970.
[28] Zhang W, Feng, G. Nonlinear Stochastic $H_2/H_{infinity}$ Control with *(x,u,v)* - Dependent Noise: Infinite Horizon Case, *IEEE Transactions on Automatic Control*, 2008; **53(5):** 1323-1328.
[29] Sheng L, Zhang W, Gao M. Relationship between Nash equilibrium strategies and H2=H1 control of stochastic Markov jump systems with multiplicative noise", *IEEE Transactions on Automatic Control*, 2014, DOI: 10.1109/TAC.2014.2309274
[30] Betts J. A survey of numerical methods for trajectory optimization, *AIAA Journal of Guidance, Control and Dynamics*, 1998; **21** (2): 193-207.
[31] Stoica AM. *Disturbance Attenuation and its Applications*, Romanian Academy Publisher, 2004.
[32] Braff R, Powell JD, Dorfler J. Applications of GPS to air traffic control, *Global Positioning System: Theory and Applications*, 1996; **II**: 327-374.